



# Digitization modeling of a CGEM detector based on Garfield++ simulation

Jing-Yi Zhao<sup>1,3</sup> · Nan-Nan Miao<sup>1,2</sup> · Ling-Hui Wu<sup>1,2</sup> · Liang-Liang Wang<sup>1,2</sup> · Tong Sun<sup>1,2</sup> · Zhen Huang<sup>1,2</sup> · Ryan Mitchell<sup>3</sup> · Wei-Guo Li<sup>1,2</sup> · Huai-Min Liu<sup>1,2</sup> · Xin-Chou Lou<sup>1,2,4</sup> · Sheng-Sen Sun<sup>1,2</sup> · Ye Yuan<sup>1,2</sup> · Yao Zhang<sup>1,2</sup>

Received: 16 December 2019 / Revised: 5 February 2020 / Accepted: 19 February 2020 / Published online: 10 March 2020  
© The Author(s) 2020

## Abstract

**Background** The Cylindrical Gas Electron Multiplier Inner Tracker (CGEM-IT) is one of the candidates for the replacement of the current BESIII inner drift chamber, which has developed serious aging effects due to beam-related backgrounds.

**Purpose** To build a full digitization model, it is necessary to understand the electron drift behavior and signal induction.

**Methods** A simulation study based on Garfield++ and ANSYS software has been performed.

**Results** Parameters describing the Lorentz angle, diffusion effect, drift time, multiplication, and induction are obtained from the Garfield++ simulation. Based on these results, a preliminary digitization model is implemented in the BESIII offline software system.

**Keywords** CGEM-IT gain · Garfield++ · Lorentz angle · Diffusion · Induction

## Introduction

The Main Drift Chamber (MDC), a key sub-detector of the Beijing Spectrometer III (BESIII), has been running for more than ten years at the Beijing Electron Positron Collider II (BEPCII). The inner part of the drift chamber, which is closest to the beam pipe, has developed serious aging effects due to the radiation from beam-related backgrounds. The gain in this region of the drift chamber has decreased year by year, causing a degradation of the hit efficiency and spatial resolution. A Cylindrical Gas Electron Multiplier (CGEM) [1] detector has been an important candidate for the upgrade of the inner tracker due to its good spatial resolution and stability in high-radiation environments.

The CGEM inner tracker [2] is designed to be composed of 3 layers of cylindrical GEM detectors. The inner radii of each layer are 76.9 mm, 121.4 mm, and 161.9 mm, and the outer radii are 90.2 mm, 134.7 mm, and 175.2 mm, respectively, as shown in Fig. 1. The length of each layer is 532 mm, 690 mm, and 847 mm, respectively. Each CGEM layer consists of a cathode, 3 GEM foils, and a readout anode, as shown in Fig. 2. The four gaps are called Drift, Transfer1, Transfer2, and Induction, with sizes of 5 mm, 2 mm, 2 mm, and 2 mm, respectively. The gas mixture is Ar/iC4H10 with a ratio of 90/10. Electric fields in the drift, transfer, and induction gaps are 1.5 kV/cm, 3 kV/cm, and 5 kV/cm, respectively. The GEM foil has a large number of double-cone shaped holes made by a single mask process using standard photolithography technology. The diameter of each hole on the foil surface is from 50 to 70  $\mu\text{m}$ , and the adjacent holes' pitch is 140  $\mu\text{m}$ , as shown in Fig. 3a. The GEM foil has a three-layer structure, i.e., two layers of copper foil with a standard thickness of 5  $\mu\text{m}$ , and a middle layer of a Kapton foil with a thickness of 50  $\mu\text{m}$ , as shown in Fig. 3b. A high voltage difference of 270 V is applied across each GEM foil. The readout anode is segmented with 650  $\mu\text{m}$  pitch XV patterned strips. The stereo angle between X and V strips changes with the layer. The electrons generated from the ionization by an incident charged particle in the gas drift toward the anode and are multiplied in the holes of the GEM foil. The moving of the

✉ Jing-Yi Zhao  
zhaoyj@ihep.ac.cn

Ling-Hui Wu  
wulh@ihep.ac.cn

<sup>1</sup> Institute of High Energy Physics, Chinese Academy of Sciences, Beijing 100049, China

<sup>2</sup> University of Chinese Academy of Sciences, Beijing 100049, China

<sup>3</sup> Indiana University, Bloomington, IN 47405, USA

<sup>4</sup> University of Texas at Dallas, Richardson, TX 75083, USA

Fig. 1 CGEM inner tracker

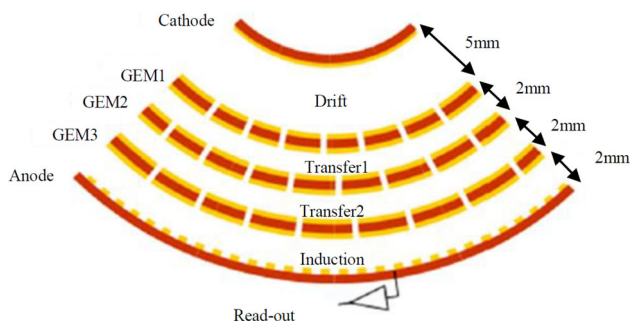
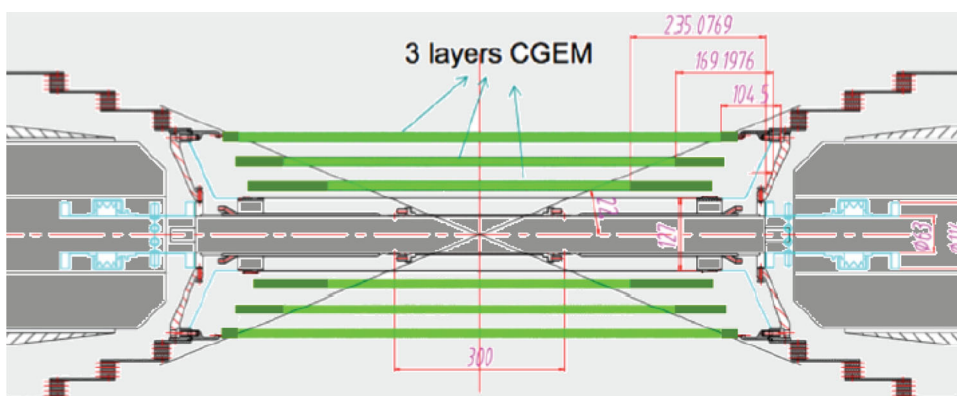


Fig. 2 Local structure of one layer of the CGEM inner tracker

electrons in the induction gap induces electrical currents in a series of anode strips, referred to as a cluster. The ionized electrons generated in the drift gap dominate the contribution to the induced signal since only these electrons are multiplied in all three GEM foils. Consequently, our digitization model only considers the ionization in the drift gap.

An analog readout is adopted for the CGEM-IT to record both time ( $T$ ) and charge ( $Q$ ) information for each firing anode strip. The position of an incident particle as it enters the drift gap can be estimated from the reconstructed cluster using  $Q$  in a charge centroid method or using  $T$  in a micro-TPC mode [3].

A Geant4-based [4] simulation of the CGEM-IT has been developed within the BESIII offline software system (BOSS

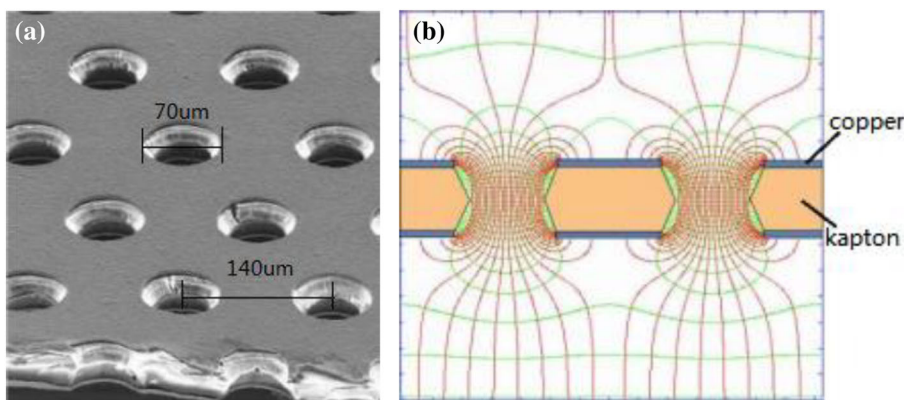
[5]. The parameters of the incident particle, including the particle type, charge, momentum, and position in the drift gap, can be obtained from the Geant4 simulation. In addition to this information, a digitization process is needed to simulate the outputs of the detector, i.e., a set of firing strips and the  $T$  and  $Q$  values for each firing strip.

The digitization process contains three steps. The first step is to simulate the ionization, which is implemented by calling the Heed package [6] through the interface provided by the Garfield++ [7] program. The second step is to simulate the drift and multiplication of the ionized and multiplied electrons. Since the complete simulation with Garfield++ of the drift line and the multiplication is time-consuming, this step is simplified by sampling the number, position, and time of the multiplied electrons. The parameters describing the Lorentz angle, multiplication, and diffusion are obtained by a prior simulation of different parts of the CGEM with Garfield++. The third step is to simulate the signal induction which is also based on a prior simulation with Garfield++ and ANSYS.

### Methods of the simulation study

The construction of the geometry of the detector and the calculation of the electric field are implemented with ANSYS

Fig. 3 a Local structure and b electric field of a single GEM foil



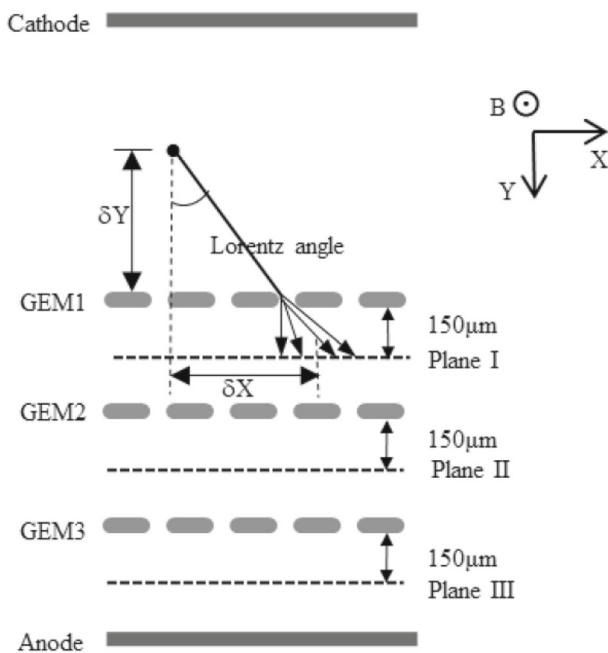


**Fig. 4** Coordinate system used in the Garfield++ simulation. The electric field is in the  $Y$  direction, and the magnetic field is in the  $Z$  direction

which is a finite element analysis software [8]. Since the drift and the avalanche of an ionized electron usually occur within a few millimeters, which is very small compared to the size of the whole detector, a planar approximation to the cylindrical shape is adopted to simplify the construction of the detector within ANSYS. The definition of the coordinates is shown in Fig. 4, where the GEM foil is perpendicular to the  $Y$  axis and the magnetic field is parallel to the  $Z$  axis. Figure 5 shows a unit of the GEM foil and a unit of the anode plane constructed within ANSYS. The field map is solved using ANSYS, which

is then used as an input for the simulation with Garfield++. Due to the periodicity of the detector structure, the CGEM detector is realized in Garfield++ by an extension of the unit structure in the  $X$  and  $Z$  axes.

The drift and multiplication of a single electron are studied with Garfield++. The method is similar to the one in reference [9], but a different parameterization method is adopted in this paper for the needs of the digitization model. As a full simulation of all drift and multiplication processes for a particle passing through the CGEM with Garfield++ is very time-consuming and hard to parameterize, it is divided into three parts. Figure 4 shows the three planes which are used in the Garfield++ simulation. A single electron is simulated as it travels from its generated position to a reference plane after the next GEM foil. This path contains the drift in one gap region and the multiplication in one layer of the foil. The distance between the reference plane and the GEM foil cannot be too small because some of the multiplied electrons may be captured by the electrode on the foil under the influence of the electric field in the region near the foil, as shown in Fig. 11. There are three reference planes, each of which is 150 microns from the GEM foil, as shown in Fig. 4. For the first part, the generated position is the location of ionization in the drift region. The electron is generated uniformly in the  $X$ – $Z$  plane with zero initial velocity. In the other two parts, the electron starts from 150 microns after the previous foil and is also generated uniformly in the  $X$ – $Z$  plane with zero initial velocity. The Penning coefficient parameter is set to be 0.44 [10] in the simulation. The parameters describing the Lorentz angle, diffusion, gain, and drift time, which will be used in the digitization model, are extracted from the simulation results of a large number of electrons.

After the drift and multiplication in the drift and transfer regions, the electron goes into the induction region. In

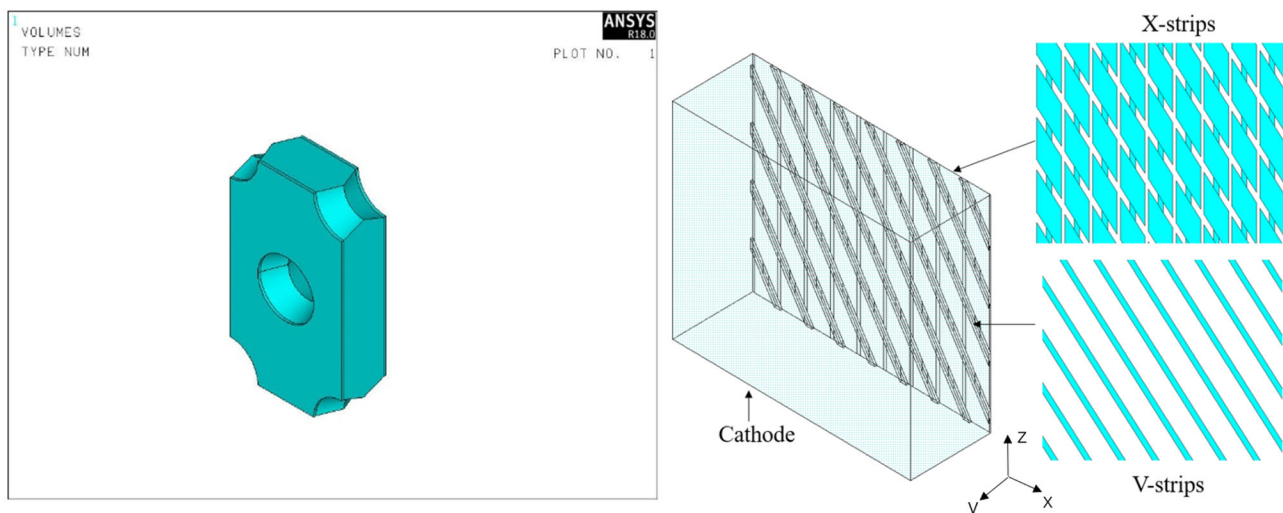


**Fig. 5** One unit of a GEM foil (left) and a unit of the anode plane (right) constructed within ANSYS

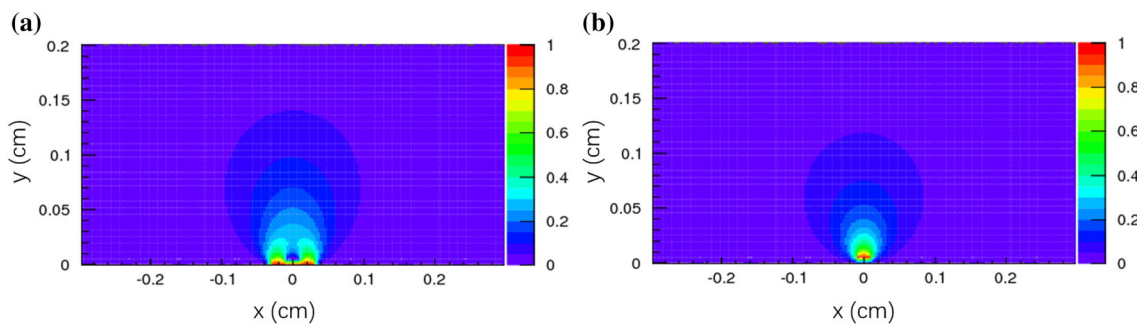


**Fig. 6** Weighting potential on **a** the central X strips and **b** the central V strips

order to make a model to simulate the induction process, a simulation study of the induced signal on anode strips was performed using ANSYS and Garfield++. The induced signal on an anode strip is described by the Shockley–Ramo theorem:

$$i(t) = -q\mathbf{v} \cdot E_w(\mathbf{r}), \tag{1}$$

where  $i(t)$  is the induced current,  $q$  is the particle charge,  $\mathbf{v}$  is the particle velocity, and  $E_w(\mathbf{r})$  is the weighting field for a given anode at particle position  $\mathbf{r}$ . The weighting field is defined as the field produced when a unit potential is applied to the readout electrode and zero potential is applied to all other electrodes [11]. The weighting field of each anode strip was calculated with ANSYS, and then it was imported into Garfield++ with the corresponding standard class to simulate the induced current on the strips. Figure 6 shows the weighting potential on the central X and V strips.

### Results of Garfield++ simulation

From the Garfield++ simulation, we can obtain the drift and multiplication behavior of a single electron, including the Lorentz angle, transverse diffusion, drift time, and electron multiplication distribution.

#### Lorentz angle

The Lorentz force causes a displacement of the electron in the X direction ( $\delta X$ ), as shown in Fig. 4. To get the Lorentz angle, the electron is generated at different Y. The distance between the electron and the top surface of the GEM foil is  $\delta Y$ . The Lorentz angle can be obtained from the line fit to the graph of  $\delta X$  versus  $\delta Y$ . Figure 7 shows the result from the drift region, and Table 1 shows the estimation of the Lorentz angle for each gap. The Lorentz angle in the drift region is bigger because of the lower electric field in this region.

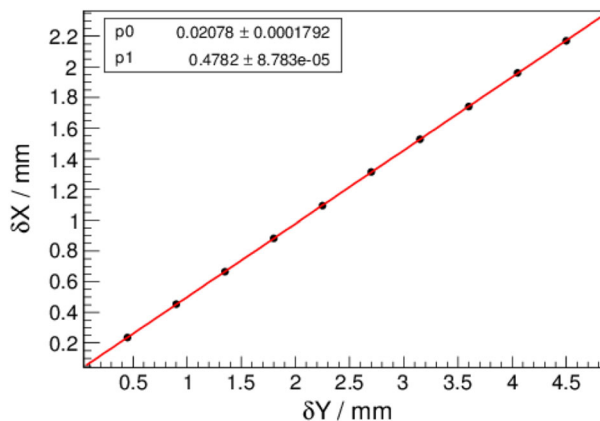


**Fig. 7** Mean displacement of multiplied electrons in the X direction ( $\delta X$ ) as a function of  $\delta Y$  for ionized electrons originating in the drift region

#### Transverse diffusion

The transverse diffusion has an impact on the cluster size of the multiplied electrons. It can be extracted from fitting the displacement distribution of the multiplied electrons, which is a Gaussian distribution. For the Transfer1 and Transfer2 regions, the diffusion effect can simply be described by the width of the Gaussian distribution since the drift distance is almost constant, as shown in Fig. 9b, c. In the drift region, the diffusion effect is a function of  $\delta Y$ , as shown in Fig. 8. Figure 9a shows the distribution of multiplied electrons with ionized electrons generated in the middle of the drift region. Table 1 shows the transverse diffusion of each region. The diffusion in the X direction is a little bigger than that in the Z direction because the drift line is not perpendicular to the X direction due to the Lorentz force.

#### Drift time

As previously mentioned in Section 2, the drift time and its resolution are functions of the drift distance in the drift

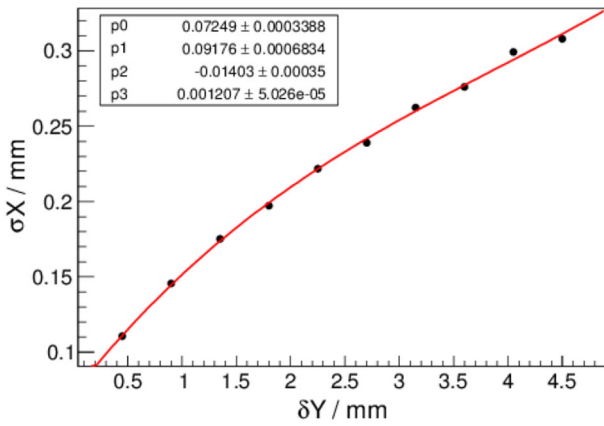


**Fig. 8** For the drift region, the Gaussian width of the multiplied electrons' displacement in the  $X$  direction as a function of  $\delta Y$

region, as shown in Fig. 10. In the Transfer1 and Transfer2 regions, because they have the same electric field, the mean of the drift time and the time resolution are very close, as shown in Table 1. Also, Table 1 shows the value of the drift time for each region.

### Multiplication

Due to the diffusion effect and the impact of the electric field on the drift line, not all the electrons can be effectively multiplied in the GEM foil. Some electrons are captured by the upper electrode before entering the hole, as shown in Fig. 11a. Some electrons are multiplied in the hole, but without multiplied electrons leaving the hole, as shown in Fig. 11b. Only the electron shown in Fig. 11c is multiplied effectively. So the multiplication of the electrons can be described with two parameters, i.e., the transparency and gain. The transparency ( $\tau$ ) is defined as:

$$\tau = N_T / N_{\text{origin}}, \tag{2}$$

where  $N_{\text{origin}}$  is the number of generated electrons, as shown in Fig. 11d, and  $N_T$  is the number of generated electrons with at least one multiplied electron reaching the reference plane below the GEM foil. The gain of electrons can be described by the Polya distribution [12]:

$$P(G) = C_0 \frac{(1 + \theta)^{(1+\theta)}}{\Gamma(1 + \theta)} \left(\frac{G}{G_0}\right)^\theta \exp\left[-(1 + \theta)\frac{G}{G_0}\right], \tag{3}$$

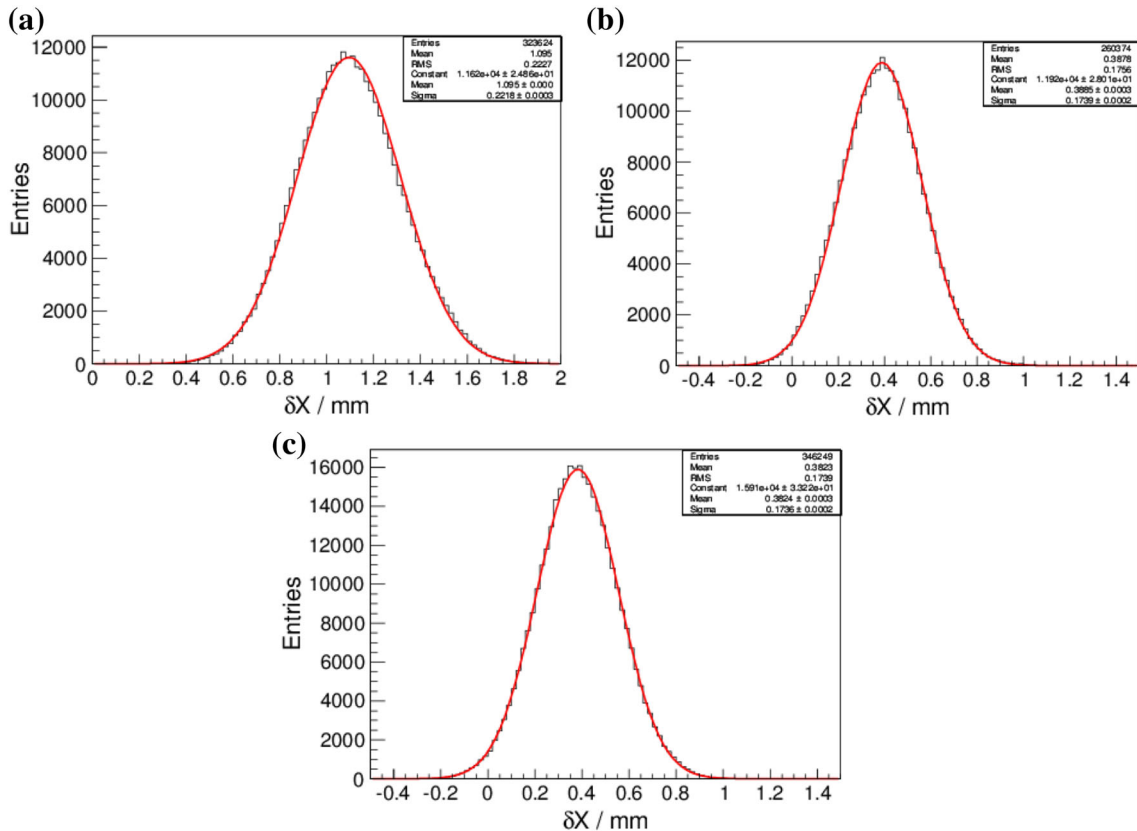


**Fig. 9** Displacement of multiplied electrons in the  $X$  direction with ionized electrons generated in **a** the middle of the drift region, **b** the Transfer1 region, and **c** the Transfer2 region

**Table 1** Parameters for the different regions

Region	Drift	Transfer1	Transfer2
Lorentz angle (degree)	25.5	10.9	10.9
$\sigma X$ (mm)	$0.0725 + 0.0918 * \delta Y - 0.0140 * (\delta Y)^2 + 0.00121 * (\delta Y)^3$	0.174	0.174
$\sigma Z$ (mm)	$0.0674 + 0.0762 * \delta Y - 0.0111 * (\delta Y)^2 + 0.00089 * (\delta Y)^3$	0.170	0.169
$T$ (ns)	$4.917 + 29.16 * \delta Y$	58.47	58.33
$\delta T$ (ns)	$0.855 + 1.116 * \delta Y - 0.202 * (\delta Y)^2 + 0.0200 * (\delta Y)^3$	2.152	2.132

**Fig. 10** For the drift region, **a** the drift time and **b** the resolution of the drift time as a function of  $\delta Y$

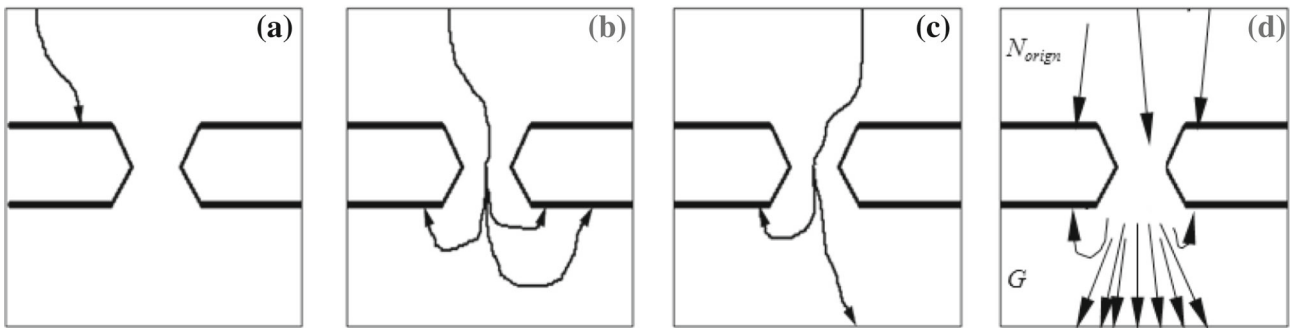
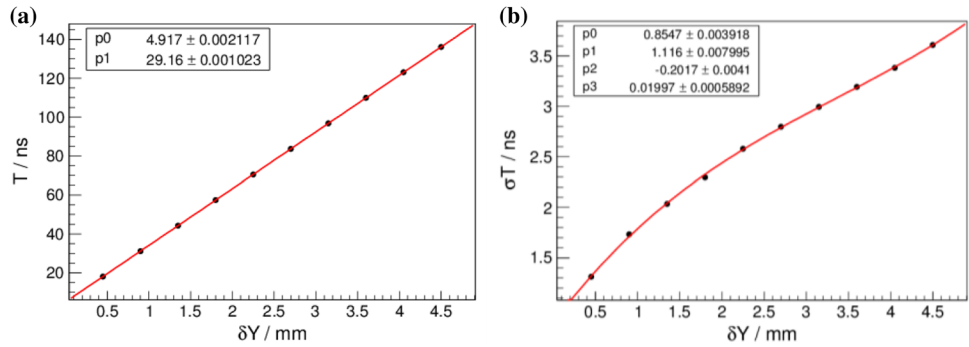
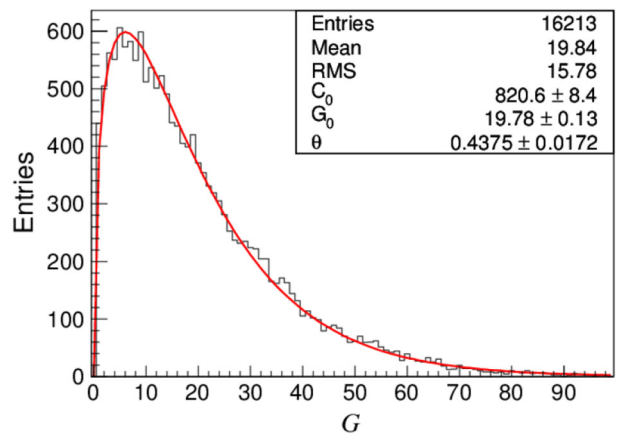


**Fig. 11** Illustration of effective GEM gain. In **a** and **b**, electrons are absorbed by the GEM foil and are not further multiplied; **c** shows an ionized electron successfully passing through the foil, and **d** shows

the number of generated electrons  $N_{origin}$  and the number of multiplied electrons,  $G$ , given that one electron passes through the GEM foil

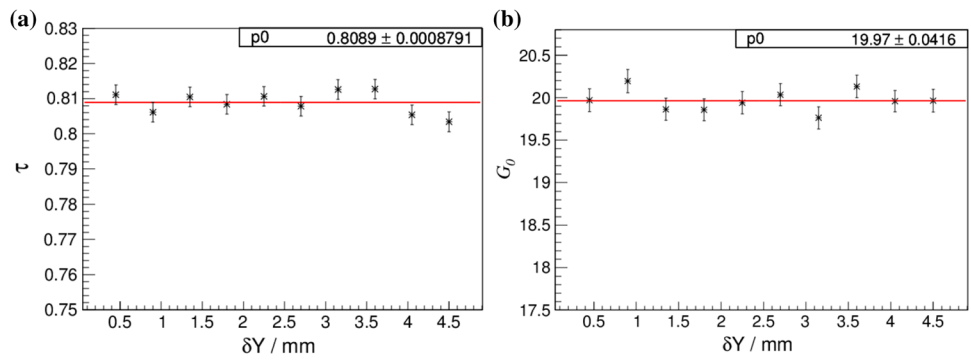
where  $C_0$  is a constant,  $G$  is the number of multiplied electrons reaching the reference plane,  $G_0$  is the average gain of a single electron, and  $\theta$  is the parameter determining the variance of the Polya distribution. The value of  $\theta$  is related to the electronic proportion of energy exceeding the ionization threshold. Figure 12 shows the distribution of  $G$  and the fit to the Polya distribution.

Figure 13 shows the  $\tau$  and  $G_0$  parameters as a function of  $\delta Y$  in the drift region, from which we see that  $\tau$  and  $G_0$  are independent of the position of the ionized electron. The  $\tau$  and  $G_0$  of the drift region are 80.9% and 20.0, respectively. Table 2 shows values of  $\tau$  and  $G_0$  for each plane. The  $\tau$  for the first GEM foil is larger than the others, because the electric field in the drift region is smaller than that in the transfer regions [13]. Both the high voltage on the GEM foil and the electric fields in the gap have an impact on  $G_0$ . Different combinations of these two factors cause different values of  $G_0$  in the different regions.



**Fig. 12** Polya distribution for GEM1 with electrons starting from the middle of the drift region and the gain measured at Plane I

**Fig. 13** **a**  $\tau$  as a function of  $\delta Y$  and **b**  $G_0$  as a function of  $\delta Y$



**Table 2** Transparency and gain for the different planes

Region	GEM foil 1	GEM foil 2	GEM foil 3
$\tau$ (%)	80.9	61.4	61.6
$G_0$	20.0	21.0	27.9

The digitization of multiplication for each GEM foil is divided into two steps. The first step is the sampling for the number of electrons that can be multiplied effectively using the transparency. The second step is the sampling of the gain with a Polya distribution.

**Signal induction**

The moving of each multiplied electron in the induction region, i.e., from the reference plane below the third GEM

foil in Fig. 4 to the anode strip, causes induced currents in several strips. The reference plane and the anode plane with both  $X$  and  $V$  strips can be divided into periodic areas. The simulation of the induction process is simplified to a small basic area. To make a fast digitization model, the basic area is divided into several grids. The induction process for electrons in each grid is simulated. The strips with induced currents and the shapes of the signals in these strips are recorded, which will be used in the digitization model. In the digitization algorithm of the induction, the final signal in each strip is the sum of the induced currents caused by all multiplied electrons. The current from each multiplied electron is obtained from the prepared record of simulated signal shapes. Figure 14 shows the final induced current on the central  $X$  and  $V$  strip when a 1.5 GeV vertical incident electron passes through the first layer of the CGEM detector.

**Fig. 14** Induced current on **a** the central  $X$  strips and **b** the central  $V$  strips

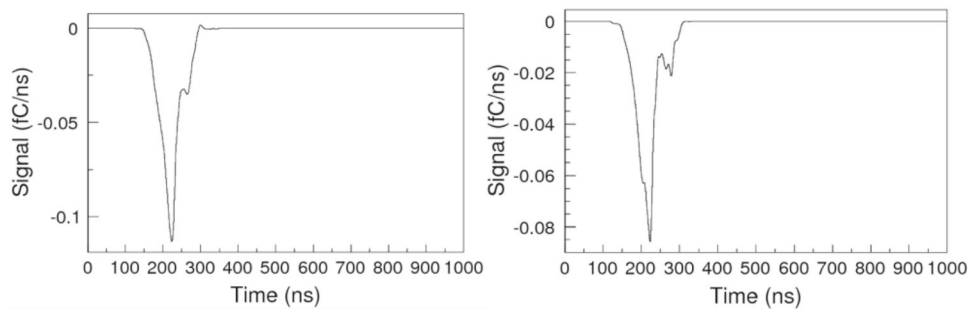
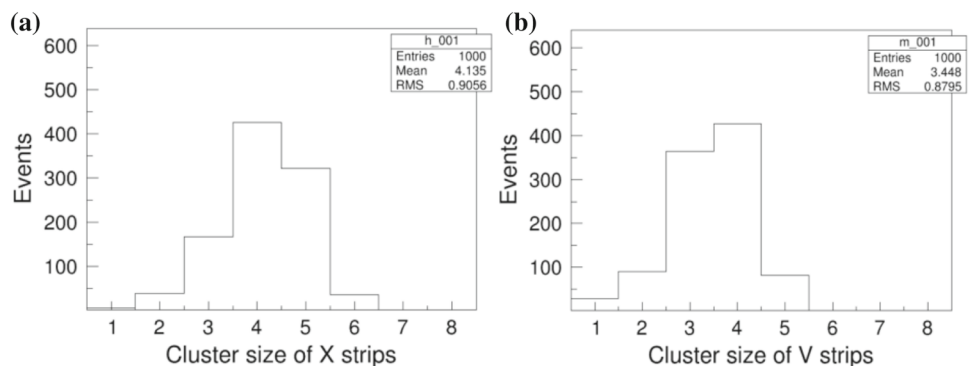


**Fig. 15** Cluster size of **a**  $X$  strips and **b**  $V$  strips



## Digitization model

Based on the results of the Garfield++ simulation described in the previous section, a preliminary full digitization algorithm has been implemented. The distribution of all the multiplied electrons after passing through the third GEM foil can be obtained from the simulation of the previous processes. Figure 15 shows the cluster size obtained from the digitization algorithm, from which we see that the mean value of the cluster size is 4.1 and 3.4 for  $X$  and  $V$ , respectively (corresponding to a stereo angle of 43 degrees between the  $X$  and  $V$  strips). The first version of the digitization algorithm has been successfully integrated into the BOSS framework. The effect of the electronics response [14] and the threshold will also be added. The procedure will be further optimized and tuned once data are collected to make the MC simulation consistent with data.

Currently, it takes a long time to run the digitization algorithm. Simulation of 100 track segments would take 1 min. The main reason is that the sampling of large number of multiplied electrons is very time-consuming. So, how to simplify the sampling process to speed up the algorithm will be considered in the next version.

## Conclusion

A simulation study using Garfield++ tool for the CGEM inner tracker has been performed according to the needs of the digitization model. Preliminary results including the Lorentz angle, diffusion, drift time, multiplication, and induction are obtained from the Garfield++ simulation and have been implemented into the digitization algorithm. Comparison with the result from the beam test [15] of the prototype shows that the cluster size from the algorithm is bigger. This difference may be due to the lack of electronic simulation and consideration of threshold effect. What is more, all parameters and settings in this work are the same as the future BESIII CGEM-IT, which are different from the prototype of beam test. Considering those factors, the cluster size from the digitization model is reasonable. The digitization model will be improved in the next step. The samplings in the process of drift and multiplication may be optimized. The difference between the experiment and simulation should be reduced after improvement and tuning with experimental data in the future.

**Acknowledgements** Funding was provided by National Natural Science Foundation of China (NSFC) under Contracts Nos. 11575222, 11475208, 11775245, 11335009, U1832204, and 11521505, National Key Basic Research Program of China under Contract No. 2015CB856706, Chinese Academy of Sciences (CAS) President's International Fellowship Initiative under Contract No. 2018PM0004, European Commission under Contract No. H2020-MSCA-RISE-2014, National 1000

Talents Program of China, and U.S. Department of Energy under Contract No. DE-FG02-05ER41374.

**Open Access** This article is licensed under a Creative Commons Attribution 4.0 International License, which permits use, sharing, adaptation, distribution and reproduction in any medium or format, as long as you give appropriate credit to the original author(s) and the source, provide a link to the Creative Commons licence, and indicate if changes were made. The images or other third party material in this article are included in the article's Creative Commons licence, unless indicated otherwise in a credit line to the material. If material is not included in the article's Creative Commons licence and your intended use is not permitted by statutory regulation or exceeds the permitted use, you will need to obtain permission directly from the copyright holder. To view a copy of this licence, visit <http://creativecommons.org/licenses/by/4.0/>.

## References

1. F. Sauli, Nucl. Instrum. Methods A **386**, 531–534 (1997). [https://doi.org/10.1016/S0168-9002\(96\)01172-2](https://doi.org/10.1016/S0168-9002(96)01172-2)
2. A. Amoroso et al., A cylindrical GEM detector with analog readout for the BESIII experiment. Nucl. Instr. Methods A **824**, 515–517 (2016). <https://doi.org/10.1016/j.nima.2015.11.082>
3. R. Farinelli, Research and development in cylindrical triple-GEM detector with TPC readout for the BESIII experiment. JINST TH **2** (2019)
4. S. Agostinelli et al., Nucl. Instrum. Methods A **506**, 250–303 (2003). [https://doi.org/10.1016/S0168-9002\(03\)01368-8](https://doi.org/10.1016/S0168-9002(03)01368-8)
5. The Offline Software for the BESIII Experiment, in *Proceeding of CHEP06* (Mumbai, India, 2006)
6. I.B. Smirnov, Modeling of ionization produced by fast charged particles in gases. Nucl. Instr. Methods A **554**, 474–493 (2005). <https://doi.org/10.1016/j.nima.2005.08.064>
7. Garfield++. <http://garfieldpp.web.cern.ch/garfieldpp/>
8. ANSYS. <https://www.ANSYS.com/>
9. W. Bonivento, A. Cardini, G. Bencivenni, F. Murtas, D. Pinci, A complete simulation of a triple-GEM detector. IEEE Trans. Nucl. Sci. **49**, 1638–1643 (2002). <https://doi.org/10.1109/TNS.2002.805170>
10. Ö. Sahin, I. Tapan, E.N. Özmütlu, R. Veenhof, JINST **5**, P05002 (2010). <https://doi.org/10.1088/1748-0221/5/05/P05002>
11. S. Ramo, Currents induced by electron motion. Proc. IRE **27**, 584 (1939). <https://doi.org/10.1109/JRPROC.1939.228757>
12. T. Zerguerras, B. Genolini, V. Lepeltier, J. Peyré, J. Pouthas, P. Rosier, Nucl. Instrum. Methods A **608**, 397–402 (2009). <https://doi.org/10.1016/j.nima.2009.07.015>
13. L. Hallermann, Analysis of GEM Properties and Development of a GEM Support Structure for the ILD Time Projection Chamber, DESY Thesis (2010). <https://doi.org/10.3204/DESY-THESIS-2010-015>
14. S. Marcello et al., The new CGEM Inner Tracker and the new TIGER ASIC for the BES III Experiment, PoS EPS-HEP2017, 505 (2017). <https://doi.org/10.22323/1.314.0505>
15. Test Beam Results of a Cylindrical GEM Detector for the BESIII Experiment, in *Proceeding of MPPGD2017, Philadelphia, USA* (2017)